X-645-73-227

PREPRINT

NASA TM X- 70444

HIGH LATITUDE ELECTRIC FIELDS AND THE MODULATIONS RELATED TO INTERPLANETARY MAGNETIC FIELD PARAMETERS

J. P. HEPPNER

JUNE 1973

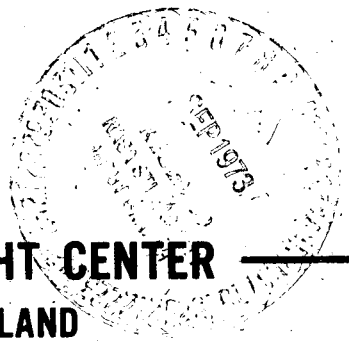

GODDARD SPACE FLIGHT CENTER
GREENBELT, MARYLAND

High Latitude Electric Fields and the Modulations Related to Interplanetary Magnetic Field Parameters

by

J. P. Heppner

Laboratory for Space Physics
NASA Goddard Space Flight Center
Greenbelt, Maryland 20771

June 1973

1. Presented at the Chapman Symposium on Magnetospheric Motions, Boulder, Colorado, June 18-22, 1973
2. For publication in Radio Science.

ABSTRACT

The meaning and characteristics of 'basic' and 'average' convection (i.e., electric field) patterns are described. The continuous existence of the basic convection pattern argues against treating magnetic field merging mechanisms as the fundamental cause of magnetospheric convection. However, whether related to merging or some other mechanism, interplanetary (IP) magnetic field conditions significantly modulate the distribution, magnitudes, and boundaries of the convection pattern. A previous correlation between azimuthal, ϕ, angles of the IP magnetic field and asymmetries in polar cap electric field distributions as seen by OGO-6 is reviewed. A new approach is taken to reveal correlations with the north-south, θ, angle and magnitude, B, of the IP field as well as additional features which correlate with the ϕ angle. Both significant correlations and conditions which show a lack of correlation are found. Several aspects of the correlations appear to be particularly important. One, is that for a given ϕ angle, correlations exist relative to θ independent of B and relative to B independent of θ. A second, is that shifts in the latitude of the low latitude limit of the auroral belt convection are strongly correlated with all parameters (ϕ, θ, B).

INTRODUCTORY DISCUSSION

Convective electric fields are apparently always present over a broad expanse of polar latitudes at ionospheric altitudes. The word "apparently" is inserted only to indicate that certainty of existence has not been established for all times and conditions. With a lesser degree of certainty, but not denied by measurements sufficiently sensitive to measure 10 volt/km fields, it also appears that the convection always follows a basic pattern in the sense of having a measurable component of anti-solar flow in a central polar cap region and east-west flows back toward the sun in both the adjacent evening and morning hours. Although the existence of a broad polar pattern at a given time can only be tested by means of spatial scans with a satellite, the numerous regional and local observations made by barium ion clouds, sounding rocket probes, radar techniques, and balloons similarly fall, collectively, into a magnetic local time and invariant latitude pattern [e.g., see reviews by Cauffman and Gurnett, 1972; Heppner, 1972a; Maynard, 1972]. The latitude-longitude tracks followed by Ba^+ clouds at a variety of high latitude locations have, in particular, been valuable in revealing the continuity characteristics of the convection on a regional scale [e.g., see Haerendel, 1972; Haerendel and Lust, 1970; Heppner, 1972a, 1972b; Heppner et al., 1971; Wescott et al., 1970].

If, based on the above statements, one assumes that a basic convection pattern always exists, it seems unlikely that the mechanism of field line merging can be regarded as the most fundamental direct cause of magnetospheric convection. This statement would not, of course, hold if it could be demonstrated: (a) that merging takes place on a large

scale at all relative angles between the interplanetary and earth magnetic fields, and (b), that the basic convection pattern is produced independent of the rates and location of the merging. Existing merging theories do not appear to satisfy either of these conditions. However, from the strong correlation recently found [Heppner, 1972d] between selected types of asymmetries in the polar cap electric field and the azimuthal direction, ϕ angle, of the interplanetary (IP) magnetic field, it is apparent that the IP magnetic field plays a significant role in the convection process. The previously presented ϕ angle correlation, and the additional correlations to be presented here, suggest that it is appropriate to view the IP magnetic field as a "modulation parameter." The correlations do not, however, reveal whether the modulating influence comes about directly through field merging or indirectly through effects on other coupling mechanisms at the magnetopause.

For relevant background information the next two sections briefly review what is meant by "basic" and "average" patterns of convection and previous attempts to find correlations with the IP magnetic field.

THE CONVECTION PATTERN

At least 5 years prior to the first high latitude $\underset{\sim}{E}$ field measurements the existence of a convection pattern was predicted by Axford and Hines [1961], Piddington [1962], and Dungey [1961]. They further, correctly predicted the basic pattern: a result which followed automatically from the assumption that auroral electrojet currents were Hall currents. By "basic pattern" one means only the existence of anti-solar polar cap flow and east-west flows back toward the sun at adjacent latitudes. A variety

of configurations can satisfy this loose definition and large deviations from the most typical configurations are indeed observed [for cross-sectional examples see, e.g., Heppner, 1972c, and the illustrative polar cap signatures in Heppner, 1972d]. However, from OGO-6 data, average locations for the boundary between the auroral belt and the polar cap and the low latitude limit of the auroral belt convection can be defined for random IP magnetic field samplings. These averages agree well with accumulated statistics from Ba^+ cloud motions and other forms of data.

Figure 1 (a) shows the idealized convection drawn by Axford and Hines [1961]. For simplicity they assumed a dipole-centered, low latitude boundary. This was placed at an equatorial distance of 4.5 R_e, corresponding to an invariant latitude of 61.9° at ionospheric levels. [Note: in this Figure and throughout the discussion, the electric field which appears in inertial coordinates as a consequence of the earth's rotation has been omitted. Also this co-rotational field, from potentials $-90 \sin^2 \theta$ kilovolts with θ = co-latitude, and V x B fields from the satellites motion, have been subtracted from the OGO-6 measurements, shown later]. Figures 1 (b) and 1 (c) are idealized illustrations of the observed convection shown in the interchangeable forms of convective flow, velocity $\underset{\sim}{V}$, and electric field, $\underset{\sim}{E}$, assuming the frozen field condition $\underset{\sim}{E} = - \underset{\sim}{V} \times \underset{\sim}{B}$. The boundary locations in Figures 1 (b) and 1 (c), except near midnight, are taken from OGO-6 averages for $K_p \doteq 3$ conditions but are idealized for analytical reproducibility by representing the polar cap-auroral belt boundary and the low latitude auroral belt boundary with two circles: respectively, a 15° radius centered at 0:00 MLT and $\Lambda = 85°$, and a 25° radius centered at 22:30 MLT and $\Lambda = 85°$ (Λ = invariant latitude). The difference between

this circular representation and actual averages is, in general, less than 2° with the maximum difference of 2° occurring near 6^h MLT. OGO-6 data, for the period of time analyzed, did not traverse the midnight meridian at $\Lambda < 70°$; the auroral belt boundary in this sector has been interpolated between earlier and later hours, primarily through the use of statistics on irregularities from the OV1-10 satellite [see, Heppner, 1972c, for an earlier representation]. The positioning of the Harang discontinuity separating east and west flows near 23^h MLT is explained in Heppner [1972b]. An equivalent boundary for the separation of east-west flows in the dayside auroral belt is not drawn. Data in this region (i.e., $\Lambda \leq 80°$ near noon)are characterized by a multiplicity of field reversals and large irregularities in the dawn-dusk component. The "turbulent" appearance of data in this region is so pronounced over such a broad area that the meaning of averages has to be treated with caution.

Several other features of the general pattern merit comment. One is that the data do not prove that the mean polar cap field is directed exactly from dawn to dusk. It could, for example, be directed normal to the meridian circle passing through 11^h and 23^h MLT without running into statistical conflict with the data. In fact, fragments of data presented for Injun-5 [Cauffman and Gurnett, 1971], Cosmos-184 [Galperin and Ponomarev, 1972], and Ba^+ cloud motions [Heppner et al., 1971] could be taken as indicating that the mean polar cap $\underline{E}$ lies more closely normal to the 11^h-23^h meridian then to the 12^h-24^h meridian. Uncertainties of this nature illustrate why Figure 1(b) is constructed in the form of flow segments without drawing the continuity of the flow.

Another feature, indicated in Figure 1(b) by the curling flow paths at the polar cap-auroral belt boundary, is that the polar cap boundary is not a shear surface. Multiple Ba^+ clouds released in the vicinity of this flow reversal have consistently shown local continuity across the boundary with changes in the direction of flow which indicate that the boundary is most typically a transition zone characterized by the presence of eddy structures. As seen in the dawn-dusk component measurements of OGO-6, the detailed appearance of the boundary varies from pass to pass; it can be either a sharp or a gradual change in the sign of the dawn-dusk component and often there are several changes in sign over dimensions ranging from tens of kilometers to several hundred kilometers. This variable appearance is what would be expected if the satellite sometimes passes through the eye of an eddy, at other times through the skirts of an eddy, and at still other times through a series of eddy structures. It appears likely that the 'inverted V' electron precipitation bands observed at this boundary by Gurnett and Frank [1973] are related to the existence of these eddy structures but this point has not been adequately examined. An example of a boundary eddy structure revealed by the time history of motion of a series of Ba^+ clouds is given in Heppner [1972a].

It has been frequently assumed that the plasmapause coincides with the low latitude limit of the high latitude convection. Thus, another feature to note in Figure 1, (b) and (c), is that this assumption does not agree with observations over a wide range of magnetic local times. Strictly on a basis of average location it appears that these two boundaries could only coincide in the late evening (e.g., MLT > 18^h) and midnight regions.

The potential drop across the polar cap, $E_3\ W_3$, where W_3 is the width of the polar cap (see Figure 1(c)), as observed by OGO-6, was generally between 20 and 100 kilovolts [Heppner, 1972c]. 100 kilovolts was exceeded in select cases. The most commonly observed values fall between 40 and 70 kilovolts under conditions of Kp = 2 to 4. Within the uncertainties imposed by the time variations that occur within the 15 to 20 minute passage over the convection pattern, and the integrated uncertainty that would result over large distances (i.e., widths W) from zero level uncertainties of 5 volts/km (imposed mainly by errors in attitude data affecting the subtraction of the $\underset{\sim}{V} \times \underline{B}$ field from satellite motion), the expected equality $E_3\ W_3 = E_1\ W_1 + E_2\ W_2$ appears to be valid.

The 3-hour magnetic disturbance index Kp is statistically related to the location of the low latitude limit of the high latitude convection. This agrees with expectation in that Kp is essentially a measure of magnetic activity at a magnetic latitude of 56° [Sugiura and Heppner, 1972] and thus depends on distance from the auroral belt. An initial analysis [Heppner, 1972c] gave the result that the low latitude boundary moved equatorward approximately 2° and 2.5°, respectively, in the MLT zones $6^h \pm 1^h$ and $18^h \pm 1^h$ for each integer increase in Kp. More complete data, now available, over a wider range of MLT will permit refinements in these figures and extension to other local times; however, it has to be recognized that individual boundary locations often deviate a number of degrees from the averages. The dependence of Kp on the integrated electric field (i.e., total potential difference) is very poorly defined. A qualitative dependence is, however, obvious from data inspection. The ranges 20 to 100 kev and Kp = 0 to 6 suggest a rough dependence in which an integer

change in Kp would accompany a 13 kev change in the total potential. A close relationship between the total potential and Kp is not necessarily expected in view of earlier findings [Wescott et al., 1970; Haerendel and Lust, 1970], subsequently confirmed by numerous examples, that there is not a close relationship between the magnitude of the surface magnetic disturbance and the magnitude of $\underset{\sim}{E}$ when observed in a localized region of the pattern. The magnitude of the magnetic disturbance is more directly dependent on ionospheric conductivity.

ASYMMETRIC POLAR CAP DISTRIBUTIONS AND THE ϕ ANGLE OF THE IP MAGNETIC FIELD

In idealizations like Figure 1, the polar cap convection is usually represented by a uniform anti-solar flow, or equivalently by a constant dawn-dusk $\underset{\sim}{E}$. However, from OGO-6 cross-sections a relatively constant $\underset{\sim}{E}$ is only one of several distributions that frequently occur. In total the dawn-dusk cross-sections have a great variety of appearances; it is, however, possible to classify practically all appearances in terms of 12 'signatures' or combinations of these signatures. Of the 12 signatures, shown in Heppner [1972d], several types of distributions have the common characteristic of being strongly skewed toward either the morning or evening hours. Examined individually, or collectively by grouping signatures, it was found that occurrences of well defined asymmetries were strongly correlated with the azimuthal angle, ϕ, of the IP magnetic field. For northern (summer) hemisphere passes it was also found that cases of uniform polar cap fields (i.e., not skewed) were correlated with the same ϕ angle sector as cases where the distribution was skewed toward a maximum in the evening hours.

An important feature of these correlations is that it was found that the asymmetries in the northern (summer) hemisphere and southern (winter) hemisphere were anti-correlated relative to the ϕ sector of the IP field. That is, asymmetrical distributions in which the southern polar cap field had a maximum in the evening hours were correlated with ϕ the same as northern polar cap fields with a maximum in the morning hours (and vice versa).

Figure 2 provides a summary of the ϕ angle correlations relative to composite signatures that represent the principal features of several more detailed signatures. [Note: the signatures shown represent the component of the electric field normal to the sun-earth line in spacecraft coordinates. In the N. hemisphere the sign of E corresponds to the sequence $E_1 \rightarrow E_3 \rightarrow E_2$ in Figure 1(c) as the satellite passes from evening to morning. In the S. hemisphere the satellite passes from morning to evening and all signs are reversed in spacecraft coordinates]. The histograms, in 45° sectors of ϕ, represent 118 polar traverses with the appropriate signatures: 84 in the northern hemisphere and 34 in the southern hemisphere. The fact that there are relatively few cases outside the principal distribution in each histogram indicates the strength of the correlation. As discussed in Heppner [1972d] it is possible that the sign of the Y component (+ Y axis at $\phi = 90^\circ$) is more significant than the value of ϕ in producing the correlation; the fact that IP magnetic field directions are predominantly either in the ϕ = 90 to 180° or 270 - 360° quadrants tends to obscure this point. A more complete discussion of the asymmetrical field correlation and its relationship to the dayside high latitude magnetic disturbance discussed by Svalgaard [1968], Mansurov [1969], and Friis-Christensen et al., [1972] is given in Heppner [1972d]. Several more recent correlations with the ϕ angle are discussed later here.

QUESTIONS RELATED TO THE θ ANGLE AND MAGNITUDE OF THE IP MAGNETIC FIELD

The correlation between polar cap distributions discussed above was found to be independent of the north-south angle, θ, and magnitude, B, of the IP magnetic field with the exception that it was noted [Heppner, 1972d] that there were minor differences in the statistical distributions of θ and B when the individual (i.e., as opposed to grouped) signatures were examined. In simple form, merging theory would predict that the polar cap flow would be the most uniform (i.e, symmetrical) when the IP field is southward (i.e., -θ). It can also be interpreted to predict the observed anti-correlation of north and south polar asymmetries relative to the ϕ angle [see, e.g., Atkinson, 1972; Jorgensen et al., 1972]. Thus the possible role of field merging in producing the ϕ angle correlations remains ambiguous.

Theories based on merging usually assume a direct relationship between the rate of convection (i.e., electric field intensity) and the rate at which IP and earth magnetic fields merge. Quantitatively, following Petschek and Thorne [1967], merging rates are usually taken to be proportional to sin $(\theta/2)$ where θ is the angle between the two fields. In developing Dungey's [1961] model of reconnection and Alfven's [1955] electric field theory it has also been popular to relate the intensity of convection to penetration of the interplanetary electric field, $-\underset{\sim}{V_i} \times \underset{\sim}{B}$ where $\underset{\sim}{V_i}$ and $\underset{\sim}{B}$ are the solar wind velocity and IP magnetic field. Correlations with magnetic activity, such as Arnoldy's [1971] finding a linear relationship between B_Z and the AE disturbance index, have been regarded as supporting this approach. However, as noted in Heppner [1969], there is an obvious difficulty with signs relative to the basic convection pattern. Thus for

a viable theory of electric field penetration it has to be related to a mechanism, such as that producing the sin $(\theta/2)$ dependence. For general reviews of these topics, see for example, Axford [1969], Nishida [1971], Nishida and Obayashi [1972], Atkinson [1972]. Particularly in treatments where the convection is related to $-\underset{\sim}{V_i} \times \underset{\sim}{B}$ it has been assumed that it is the total potential (i.e., integrated $\underset{\sim}{E}$) within the magnetosphere that should show a correlation with the interplanetary $\underset{\sim}{B}$. The arguments are, however, highly qualitative. It appears that relative to open magnetospheric models there is also the possibility that merging proceeds rapidly only in localized areas of the magnetopause. In this case regional details within the convection pattern might correlate with the interplanetary $\underset{\sim}{B}$.

The above discussion, centered on open magnetosphere merging models, illustrates that even though the existence and asymmetries of the convection pattern appear to be independent of θ and B, there is a need to examine relationships with integrated electric fields, peak magnitudes and other defined quantities such as boundary locations. Relative to theories of viscous interaction at the magnetopause, non-merging mechanisms for particle entry, hydromagnetic wave coupling, etc., models which would predict dependence on IP magnetic field conditions have not been developed. Thus in seeking correlations one is not testing existing models; instead the search is for guidelines for the future development of ideas.

TESTS FOR θ and |B| DEPENDENCE

Visual Examination

The existence of the ϕ angle correlations of Figure 2, discussed earlier, was obvious from visual examination of data even though a signature classification was required to see the strength of the correlation. The fact that correlations with θ and B are not visually obvious is, in itself, indicative that major differences in the convection related to the north-south component of $\underset{\sim}{B}$ are not as likely to appear in analyses. Figures 3 and 4 illustrate this point. These examples are chosen for their relatively constant ϕ angle conditions and similarity of cross-sectional asymmetrical signatures in the polar cap such that variations between successive polar passes can be examined relative to changes in the θ angle. The black rectangles on the B, ϕ, θ records correspond to the simultaneous time intervals of the OGO-6 E_X data. As Explorer-33 was located, relative to the noon magnetopause, at an angle approximately equal to the average spiral angle at 1 AU for a radial solar wind, a time difference between the two sets of data has not been included to try to optimize correlation possibilities.

Figure 3 shows two successive OGO-6 traverses with similar E_X latitudinal profiles (corresponding to signature RC in Heppner, 1972d). The simultaneous ϕ and B values are roughly equal in the two cases but θ changes from slightly northward to values of -60 to -70°. The principal difference is that $-E_X$ on the morning side of the polar cap has a greater magnitude in the case of the southward IP magnetic field. Some fraction of this difference could result from the second pass being more polar in magnetic coordinates than the first pass.

Figure 4 shows five successive traverses with related asymmetric signatures (corresponding to SC and combinations of B and G in Heppner, 1972d). ϕ remained in the same quadrant through this series and there were only small changes in B. Even with allowance for orbital differences and a possible 5 volt/km error in the zero baseline, the integrated E_x in passes 4 and 5 appears greater than for passes 1-3. Passes 4 and 5 occur during the most southward IP magnetic field. However, it should also be noted that pass 3 with a northward IP field more closely resembles passes 4 and 5 than pass 1 which also occurred with a southward field. Some differences here are probably related to the cross-sections occurring sequentially from the dayside to the nightside of the 18^h-6^h meridian. A point to note, relative to later discussion, is that the low latitude boundary of the auroral belt convection appears to spread southward in passes 4 and 5.

The above examples do not prove anything. Their purpose is to illustrate: (a) that one needs to look at details to test for the significance of southward IP fields, and (b) that even in simple cases these details can be influenced by the location of the traverse in magnetic coordinates.

Integrated E_x (Potential Drop)

Relative to model expectations, discussed previously, and examples like Figure 4, one would logically seek correlations between the IP field and the total potential drop across the polar cap or the two auroral belts. Thus, the fact that this is not done here requires explanation. Missing data segments within individual passes present one problem which restricts the OGO-6 statistics to passes where the complete line integral

is obtained. Passes for which the IP data is missing are also eliminated. Significant numbers would still be available but these lose significance in the face of two more fundamental problems. One is that because of the varied paths in magnetic coordinates, individual passes have to be compared with a model rather than directly with each other. This introduces a model uncertainty. The other problem is that the uncertainty in the baseline for $E_x = 0$ is about 5 volts/km and this uncertainty is a variable from orbit to orbit as it is related to uncertainties (e.g., up to 2°) in the orientation of the spacecraft that affect the subtraction of the $\underset{\sim}{V} \times \underset{\sim}{B}$ field from satellite motion. When integrated over 30° a 5 volt/km uncertainty becomes a 17 kev uncertainty in the potential drop.

Using reasonable assumptions to compensate for uncertainties the above problems would not be an obstacle to analysis if the dependence on θ and/or B was large and the integrated E_x was also independent of ϕ. However, simply from inspection one does not expect large differences as a function of θ and/or B, and as shown in subsequent analysis both integrated averages for E_x and peak magnitudes are not statistically independent of ϕ.

Bohse and Aggson [1973] avoided the missing data problem, and hopefully averaged out uncertainties, by averaging all OGO-6 data for $\Lambda > 45°$ using a 2° grid. The contoured average values were then integrated. Relative to Explorer-35 B, θ, ϕ data plots, average fields were constructed separately for + and - θ, B = 2 to 6$^\gamma$ and 6 to 12$^\gamma$, and ϕ = 0 - 180° and 180° - 360° (i.e., + and $-B_y$). The polar cap potential drops were 44 and 53 kev, respectively, for plus (northward) and minus (southward) θ, and 45 and 53 kev, respectively, for B values of 2 to 6$^\gamma$ and 6 to 12$^\gamma$. In

recognition of the asymmetries which correlate with ϕ, the averaging and grouping of northern and southern hemisphere data was performed both for B_y having the same and opposite signs in the two hemispheres. This gave the ranges 42 to 48 kev for + B_y (i.e., $\phi = 0° - 180°$) and 57 to 58 kev for - B_y (i.e., $\phi = 180° - 360°$). These gross averages, and thus their physical meaning, can be readily criticized on grounds that the variables are not separated and also on grounds that shifts in the position of the polar cap-auroral belt boundary will produce average values for $|E_x|$ that are less than the values in individual cases over the range of latitudes of boundary shifting. Nevertheless, each of the above results is consistent with the findings described below which are based on a technique designed specifically to separate variables and also to examine boundary shifts as a function of the variables.

Extremes Compared with Averages

This section describes a technique for testing the dependence of boundary locations and peak magnitudes on IP field parameters with the minimum amount of mixing of variables that appears achievable within the limited statistics. The principal limitation of this technique is that it produces small sample statistics such that some isolated results cannot be considered statistically meaningful and must be grouped for interpretation.

First, only OGO-6 polar traverses which fall completely in the band bounded by $18^h \pm 1^h$ and $6^h \pm 1^h$ magnetic local time above $\Lambda = 60°$, shown in Figure 5, are considered. This not only restricts the sampling to similar traverses but also limits the sampling to a reduced range of tilt angles between the earth's dipole field and the IP magnetic field: corresponding to ranges in UT of < 9 to < 5 hours per day over the range

of dates involved, June 10-22, 1969. The orbit inclination is such that these hours are the same for northern (summer) and southern (winter) hemisphere traverses [see Heppner, 1972c for the orbit and data distribution characteristics]. Boundary data are further sub-classified to separate $17\text{-}18^h$ from $18\text{-}19^h$ MLT and $6\text{-}7^h$ from $5\text{-}6^h$.

Second, for each polar pass median values of θ, ϕ, and B for 30 minute time intervals were read to determine the median location within six 30° increments of θ, eight 45° sectors of ϕ, and 2γ increments of B. This was done for both $-15^m < T < 15^m$ and $-45^m < T < -15^m$ where T is the time, to the nearest minute, when OGO-6 was at the maximum invariant latitude for that pass. Only Explorer-33 interplanetary field, $\underset{\sim}{B}_{ip}$, data in solar-equatorial coordinates were used to avoid any measurement differences and uncertainties in correcting for propagation time (e.g., the less complete Explorer-35 data could have been used to fill missing intervals in the Explorer-33 data but this would have introduced a timing variable).

Next, data were separated for $90^\circ < \phi < 180^\circ$ and $270^\circ < \phi < 360^\circ$ and data taken when ϕ was not in one of these two sectors were not used. Figure 5 illustrates the total distribution of data for $-15^m < T < 15^m$ and $-45^m < T < -15^m$.

Analyses to look for boundary location and peak magnitude effects are then based on comparing values in the 'wings' of the distributions ($\theta < -30^\circ$, $\theta > 30^\circ$, $B < 4\gamma$ and $B > 8\gamma$) with average values for the same conditions: $90^\circ < \phi < 180^\circ$ or $270^\circ < \phi < 360^\circ$, $-15^m < T < 15^m$ or $-45^m < T < -15^m$, summer or winter hemisphere, magnetic local times $17\text{-}18^h$ or $18\text{-}19^h$ or $6\text{-}7^h$ or $5\text{-}6^h$. Examination of Tables 1-3, discussed in the next section, will further clarify this procedure.

As the θ and B wings are analyzed independently, one needs to know the extent to which samples occurring in a wing of the θ distribution also occur in a wing of the B distribution, and vice versa. As an example 13% of the samples that fall in the wing for $B > 8^{\gamma}$ also occur in the wing $\theta > 30^{\circ}$. The eight percentages for the four wings are 4, 5, 8, 8, 11, 13, 13, and 14. Thus there is not extensive overlap. As an average, if 10 or 11 samples give a correlation relative to one wing (e.g., in B) only one of these samples will be contributing to the same correlation if it appears in a wing of the other parameter (e.g., in θ); furthermore, this small effect is offset relative to a common correlation by the fact that it is also likely that one of the 10 or 11 samples will occur in the opposite wing of the other parameter. It is important to recognize that the overlap of wings is both small and relatively random as the results, discussed next, indicate that θ and B correlations are very similar.

BOUNDARY LOCATIONS AND PEAK MAGNITUDES CORRELATED WITH θ and B

Results from the analysis described in the previous section are presented in Tables 1-3 in the form of testing a series of statements. A percentage of 100 indicates complete agreement (i.e., correlation), 50 indicates the absence of either agreement or disagreement (i.e., lack of correlation), and 0 indicates complete disagreement (i.e., anti-correlation). Explanation of the first line and first columns (i.e., for $\theta < -30^{\circ}$) of Table 1 will illustrate the procedure. This says that there were 83 polar cap-auroral belt boundary crossings within the time-latitude zone sampled in the northern (summer) hemisphere for which IP magnetic field data was available for the time interval $-15^{m} < T < 15^{m}$. Nine (9) of these crossings occurred when the IP field was more than 30° southward.

In 6 of the 9 cases (i.e., 67%) the polar cap-auroral belt boundary was at a lower latitude than the average latitude for all cases occurring when ϕ was in the same quadrant and the traverse was across the same hour in MLT. The second line of Table 1 illustrates another point that requires explanation in that it shows that there were 96 boundary crossings for which IP magnetic field data was available for the time interval $-45^m < T < -15^m$; this difference, 96 as compared to 83, is solely the consequence of there being more occasions when IP data was missing between $-15^m < T < 15^m$ than during $-45^m < T < 15^m$ for the data on crossings of this boundary. Another point requiring explanation is that results for evening and morning boundary crossings and evening and morning auroral belt peak magnitudes, have been lumped together in Tables 1 and 2, respectively. Separate evening and morning tables were constructed but differences which could be treated as being statistically significant were not found; hence they were lumped to save space. The possibility that more extensive statistics would show meaningful differences between morning and evening data as a function of θ and B is not ruled out.

Polar Cap-Auroral Belt Boundary

In general, but with one obvious exception, Table 1 indicates a lack of correlation between the latitude of the polar cap boundary and θ and B. The exception is the summer hemisphere case where the field is southward prior ($-45 < T < -15$) to the polar pass. The other three conditions, rather vaguely, also indicate a greater chance of correlation relative to the time interval $-45 < T < -15^m$. The winter (southern) polar boundary data (Table 1: marked with an asterisk) cannot be interpreted because a large number of these boundaries involved multiple field reversals and were omitted. The

fact that the winter polar cap boundary in this MLT range is often highly complex is illustrated in Heppner [1972c]; a satisfactory explanation for this difference between the summer and winter polar regions has not been developed. The related subject of winter polar cap field irregularities is discussed later in this paper.

Auroral Belt Low Latitude Boundary

Table 1 shows that the low latitude limit of the auroral belt convection in the summer hemisphere strongly correlates with both θ and B. A weaker correlation appears in the winter hemisphere. A reason for this difference between hemispheres is not obvious; there could be some influence from the fact that zero levels for E_x appear to be more in error in the southern hemisphere than in the northern hemisphere, as stated in Heppner [1972c], but the picking of boundary locations utilizes data channels that reveal gradients and irregularities in the field in addition to the d.c. data channels. Also the margin for error in locating this boundary on individual passes should be the same for all passes as the scaling of OGO-6 data was performed independent of all other forms of data.

Shifts in the latitude of this boundary appear to be equally well correlated with θ and B and the time intervals $-15 < T < 15$ and $-45 < T < -15$.

Peak Magnitudes in the Polar Cap

The small numbers in Table 2 are not statistically significant for isolated ϕ and θ or ϕ and B conditions. However, the numbers become significant when grouped. A definite correlation appears when the southern (summer) hemisphere samples for the simultaneous time interval, $-15 < T < 15$, are grouped for the four θ and B columns. When this is done 17 of 18 cases agree with the statements being tested. Thus it appears safe to state that

there is a strong correlation between peak magnitudes in the summer polar cap and the simultaneous θ and B.

The same correlation is not apparent in the winter polar region where the identical grouping shows only 10 of 17 cases in agreement with the statements; however, 6 out of 7 are in agreement if only the sector $90^\circ < \phi < 180^\circ$ is considered.

With the exception of the summer polar cap for $90^\circ < \phi < 180^\circ$ there is a general lack of correlation relative to θ and B values which existed prior ($-45^m < T < -15^m$) to the satellite traverse.

Peak Magnitudes in the Auroral Belt

Table 3 clearly shows a correlation with auroral belt peak magnitudes in the summer hemisphere for the azimuthal sector $270^\circ < \phi < 360^\circ$. For the same sector results are indefinite in the winter hemisphere. Except for conditions of very weak fields, $B < 4\gamma$, there is a lack of correlation for the sector $90^\circ < \phi < 180^\circ$ in both the summer and winter hemispheres. Less than average peak magnitudes occur for all cases of $B < 4\gamma$.

ADDITIONAL ϕ ANGLE CORRELATIONS

The tabulations of boundary locations and peak magnitudes used for examining θ and B correlations, above, provide additional information on ϕ dependencies, discussed previously, and in Heppner [1972d]. In Heppner [1972d] it was stated that shifts in the polar cap-auroral belt boundary accompanied the asymmetric distributions and a 3° shift was used for illustration. Average shifts for combinations of the two hemispheres and different MLT hours ranged from 2° to 5° in the present analysis. These were in the same direction as shown in the previous analysis.

The low latitude boundary of the auroral belt convection does not shift in synchronism with shifts in the polar cap-auroral belt boundary. Instead, for the total data sample (i.e., essentially random θ and B conditions), this boundary statistically occurs at a lower latitude for $270^\circ < \phi < 360^\circ$ than for $90^\circ < \phi < 180^\circ$. The 16 averages (from 2 hemispheres, 4 hours of MLT, and time intervals $-45^m < T < -15^m$ and $-15^m < T < 15^m$) give relative shifts for the two ϕ quadrants ranging from 0° to 5°. In the majority of cases the boundary is 2° to 3° lower in latitude for $270^\circ < \phi < 360^\circ$ than for $90^\circ < \phi < 180^\circ$.

Table 4 gives statistics on peak magnitudes for the total data sample independent of θ and B conditions. The larger peak magnitudes in the winter, than in the summer, hemisphere relate to the more irregular field in the winter hemisphere, as noted in Heppner [1972c]. They do not imply that there is any difference in the integrated E-field in the two hemispheres. Bohse and Aggson [1973] found the two (north and south) integrated fields to be essentially equal for averaged data. As a consequence of the influence of irregularities in the winter hemisphere the small differences between $90^\circ < \phi < 180^\circ$ and $270^\circ < \phi < 360^\circ$ may not be meaningful. The fractionally larger differences that appear in the summer hemisphere auroral belt are, however, significant. These show an average increase of 30 to 50% in peak magnitudes in switching from $90^\circ < \phi < 180^\circ$ to $270^\circ < \phi < 360^\circ$. This difference is independent of θ and B; however, as noted previously (Table 3) there is an additional correlation with θ and B for $270^\circ < \phi < 360^\circ$ that does not appear to exist for $90^\circ < \phi < 180^\circ$.

WEAK SUMMER AND IRREGULAR WINTER FIELDS

From visual examination of OGO-6 data it was apparent that passes showing very weak fields in the northern hemisphere and passes showing highly irregular fields in the southern hemisphere often occurred on the same orbit. As this suggested that the two quite different behaviors might relate to a common cause,the IP magnetic field conditions were examined. First, by a process of selection and elimination, involving only passes where there were not significant data gaps, it was possible to isolate 13 northern and 12 southern passes as showing, respectively, the "weakest integrated E-field" and the "greatest degree of E-field irregularity in the polar cap." In selecting the southern (winter) irregularity cases the additional condition of selecting only from passes on the nightside of the 18^h-6^h meridian was imposed to avoid conflict with possible selection of normal polar cusp conditions. "Degree of irregularity" is only qualitatively defined; essentially it means numerous field reversals and large amplitude changes in the dawn-dusk component over dimensions of tens to hundreds of kilometers as opposed to the several thousand kilometer dimensions that usually define the polar cap. Thus, the irregularity fields are strong fields; however, because of the frequent sign reversals the line integral in these cases gives a small total potential drop across the polar cap.

Figure 6 illustrates the B, θ, and ϕ conditions accompanying these cases. The histograms include conditions for both time intervals: $-45^m < T < -15^m$ and $-15^m < T < 15^m$. It is immediately obvious that the B and θ distributions accompanying these cases are shifted toward small B and northward θ angles relative to the distribution of all data. However, although not as obvious until carefully examined, it is probably equally

or more meaningful that the ϕ distribution is also changed. In particular, the normal 90° - 180° distribution collapses to the range 135° - 180°, the 270° - 360° distribution collapses to 315° - 360°, and a higher percentage than normal appears in the 45° sectors 180° - 225° and 0° - 45°. That is, the distribution is strongly biased toward IP magnetic fields directly toward or away from the sun with an additional preference for the away, 180°, direction.

A physical interpretation of the different, northern and southern, field behaviors is not attempted here. Relative to other IP field correlations these cases are in general agreement but illustrate several points: one, that similar correlations with the IP field for polar cap peak magnitudes in summer and winter should not be expected (Table 2); second, that a complete separation of variables is not possible in a 3-dimensional picture; and third, that with larger statistics it is likely that correlations with the ϕ angle could be made more explicit in terms of sectors smaller than 90°.

SUMMARY COMMENTS

Table 5 summarizes the relationships found in looking for correlations with θ and $|B|$ by separating the variables and examining differences between average conditions and conditions present for $B < 4\gamma$, $B > 8\gamma$, $\theta > 30°$, and $\theta < -30°$. This table together with both the new and previously found correlations with the azimuthal, ϕ, angle of the IP magnetic field illustrate that there are complex differences between conditions which correlate and conditions which do not correlate. A few generalizations are, however, possible.

(a) Asymmetric polar cap distributions, auroral belt-polar cap boundary shifts in the dawn-dusk direction, the latitude of the low latitude boundary of the auroral belt convection, and peak magnitudes in the auroral belt, all show relationships with the ϕ angle. The existence of correlations between peak magnitudes and θ and B also depends on the ϕ angle.

(b) Shifts in the latitude of the low latitude boundary of the auroral belt convection occur as a function of θ or B for both ϕ sectors.

(c) Although there are conditions which show a lack of correlation relative to theoretical expectations involving the importance of strong southward IP magnetic fields, statistically significant categories of anti-correlation were not found. However, the correlations which exist relative to the magnitude, B, independent of θ do not support expectations that the B_z component determines the correlation.

In addition to the above generalizations the results in total suggest that the auroral belt parameters respond more directly than the polar cap parameters to different θ and B conditions. This is a characteristic that is likely to be of importance in eventual interpretation. As an example, in terms of existing merging models it is not at all apparent why the location of the low latitude boundary of the auroral belt convection should be the most highly correlated parameter. The author's immediate impression is that this is indicative of hydromagnetic wave coupling but for the present this impression is purely speculative. As a note of caution in applying interpretations to the correlations presented, it should be kept in mind

that it is automatically assumed that the solar wind density and velocity are constant. Correlative variations and relationships between the solar wind plasma and the IP magnetic field could affect the analysis.

TABLE TITLES

Table 1: Tests of statements 1-4 regarding the dependence of boundary locations on $\underset{\sim}{B}_{ip}$.

Table 2: Tests of statements 1-4 regarding the dependence of polar cap peak magnitudes on $\underset{\sim}{B}_{ip}$.

Table 3: Tests of statements 1-4 regarding the dependence of auroral belt peak magnitudes on $\underset{\sim}{B}_{ip}$.

Table 4: Average peak magnitudes for passes between 18 ± 1^h and 6 ± 1^h MLT (Units: millivolts/meter).

Table 5: Summary of correlations with θ and $|B|$ found by comparing conditions for $B < 4^\gamma$, $B > 8^\gamma$, $\theta > 30^\circ$, and $\theta < -30^\circ$ with averages.

FIGURE CAPTIONS

Figure 1: (a) Axford-Hines model convection, (b) characteristic convection from observations, and (c) characteristic directions of the observed electric field. In (b) and (c) average boundaries for the low latitude limit of the auroral belt convection and the transition from polar cap to auroral belt convection are modelled with two off-axis circles for Kp $\triangleq$ 3 conditions. Coordinates are magnetic local time and invariant latitude.

Figure 2: Histograms for the ϕ angles of the IP magnetic field accompanying occurrences of selected types of dusk-dawn (N. Hemi.) and dawn-dusk (S. Hemi.) electric field distributions in the polar caps (from Heppner, 1972d).

Figure 3: OGO-6 electric field measurements from two successive northern high latitude passes and Explorer-33 IP magnetic field data in solar-equatorial coordinates.

Figure 4: OGO-6 electric field measurements from five successive northern high latitude passes and simultaneous Explorer-33 IP magnetic field measurements.

Figure 5: Histograms for the IP magnetic field parameters ϕ, θ, and B accompanying OGO-6 passes which fall completely within the shaded area (upper left) above $\Lambda = 60^{\circ}$. Shaded areas in the ϕ, θ, B histograms were used for analysis.

Figure 6: B, θ, and ϕ histograms for comparing distributions accompanying selected conditions with distributions for the total sample.

ACKNOWLEDGMENTS

The Explorer-33 magnetic field data was available at the NASA National Space Science Data Center through the efforts of Dr. D. S. Colburn, NASA Ames Research Center. A number of GSFC co-workers have made this analysis possible; particular credit is due co-investigators Drs. T. L. Aggson and N. C. Maynard.

REFERENCES

Alfvén, H. (1955), On the electric field theory of magnetic storms and aurorae, Tellus, 7, 50-64.

Arnoldy, R. L. (1971), Signature in the interplanetary medium for substorms, J. Geophys. Res., 76, 5189-5201.

Atkinson, G (1972), Magnetospheric flows and substorms, pp. 203-216, Magnetosphere-Ionosphere Interactions (ed. by K. Folkestad) Universitetsforlaget, Oslo.

Axford, W. I. and C. O. Hines (1961), A unifying theory of high-latitude geophysical phenomena and geomagnetic storms, Can. J. Phys., 39, 1433-1463.

Axford, W. I. (1969), Magnetospheric convection, Rev. Geophys, 7, 421-459.

Bohse, J. R. and T. L. Aggson (1973), Average ionospheric electric field distribution, EOS (Abstract), Trans. Amer. Geophys. Union, 54, 417.

Cauffman, D. P. and D. A. Gurnett (1971), Double-probe measurements of convection electric fields with the Injun-5 satellite, J. Geophys. Res., 76, 6014-6027.

Cauffman, D. P. and D. A. Gurnett (1972), Satellite measurements of high latitude convection electric fields, Space Sci., Rev., 13, 369-410.

Dungey, J. W., (1961), Interplanetary magnetic field and the auroral zones, Phys. Rev. Letters, 6, 47-48.

Galperin, Yu. I. and V. N. Ponomarev (1972), Direct measurements of plasma convection in the upper ionosphere (preprint).

Gurnett, D. A. and L. A. Frank (1973), Observed relationships between electric fields and auroral particle precipitation, J. Geophys. Res., 78, 145-170.

Haerendel, G. (1972), Plasma drifts in the auroral ionosphere derived from barium releases, pp. 246-257, Earth's Magnetospheric Processes (ed. by B. M. McCormac) D. Reidel Publ. Co., Dordrecht-Holland.

Haerendel, G. and R. Lust (1970), Electric fields in the ionosphere and magnetosphere, pp. 213-228, Particles and Fields in the Magnetosphere, (ed. by B. M. McCormac), D. Reidel Publ. Co., Dordrecht-Holland.

Heppner, J. P. (1969), Magnetospheric convection patterns inferred from high latitude activity, pp. 251-266, Atmospheric Emissions (ed. by B. M. McCormac and A. Omholt) Van Nostrand Reinhold Co., New York.

Heppner, J. P. (1972a), Electric fields in the magnetosphere, pp. 107-122, Critical Problems of Magnetospheric Physics (ed. by E. R. Dyer) IUCSTP Secretariat, National Academy of Sciences, Washington, D. C.

Heppner, J. P. (1972b), The Harang discontinuity in auroral belt ionospheric currents, Geofysiske Publikasjoner, 29, 105-120.

Heppner, J. P. (1972c), Electric field variations during substorms, Planet. Space Sci., 20, 1475-1498.

Heppner, J. P. (1972d), Polar cap electric field distributions related to the interplanetary magnetic field direction, J. Geophys. Res., 77, 4877-4887.

Heppner, J. P., J. D. Stolarik, and E. M. Wescott, (1971), Electric field measurements and the identification of currents causing magnetic disturbances in the polar cap, J. Geophys. Res., 76, 6028-6053.

Jorgensen, T. S., E. Friis-Christensen, and J. Wilhjelm (1972), Interplanetary magnetic field direction and high-latitude ionospheric currents, J. Geophys. Res., 77, 1976-1977.

Maynard, N. C. (1972), Electric fields in the ionosphere and magnetosphere, pp. 155-168, Magnetosphere-Ionosphere Interactions (ed. by K. Folkestad) Universitetsforlaget, Oslo.

29

Nishida, A. (1971), Interplanetary origin of electric fields in the magnetosphere, Cosmic Electrodynamics, 2, 350-374.

Nishida, A. and T. Obayashi (1972), Magnetosphere convection, pp. 179-194, Critical Problems of Magnetospheric Physics (ed. by E. R. Dyer) IUCSTP Secretariat, National Academy of Sciences, Washington, D. C.

Petschek, H. E. and R. M. Thorne (1967), The existence of intermediate waves in neutral sheets, Astrophys. J., 147, 1157-1163.

Piddington, J. H. (1962), A hydromagnetic theory of geomagnetic storms and auroras, Planet. Space Sci., 9, 947-957.

Sugiura, M. and J. P. Heppner (1972), Electric and magnetic fields in the earth's environment, Chapter 5, pp. 264-303, Amer. Inst. of Phys. Handbook (3rd edition), McGraw Hill Book Co., New York.

Wescott, E. M., J. D. Stolarik, and J. P. Heppner (1970), Auroral and polar cap electric fields from barium releases, pp. 229-238, Particles and Fields in the Magnetosphere (ed. by B. M. McCormac), D. Reidel Publ. Co., Dordrecht-Holland.

TABLE 1: Tests of statements 1-4 regarding the dependence of boundary locations on $\underset{\sim}{B}_{ip}$

1. Southward B_{ip} shifts polar cap and auroral belt boundaries to lower latitudes.
2. Northward " " " " " " " " higher latitudes.
3. Strong " " " " " " " " lower " .
4. Weak " " " " " " " " higher " .

Boundary locations for $\theta < -30^\circ$, $\theta > 30^\circ$, $B > 8\gamma$, and $B > 4\gamma$ compared with the average locations for the same combinations of: magnetic local time ($17\text{-}18^h$ or $18\text{-}19^h$ or $5\text{-}6^h$ or $6\text{-}7^h$) and, ϕ_{ip} sector ($90^\circ < \phi < 180^\circ$ or $270^\circ < \phi < 360^\circ$)

	N Total	N $\theta < -30^\circ$	agree	%	N $\theta > 30^\circ$	agree	%	N B>8	agree	%	N B<4	agree	%
Polar Cap-Auroral Belt													
(A) Summer pole													
-15 < T < 15	83	9	6	67	10	4	40	9	5	56	2	0	0
-45 < T < -15	96	14	13	93	9	6	67	8	5	63	9	4	44
(B) Winter pole													
-15 < T < 15	54*	12	6	50*	0	-	-*	9	5	56*	2	1	50*
-45 < T < -15	49*	11	4	36*	3	2	67*	4	1	25*	6	3	50*
Auroral Belt Lower Edge													
(A) Summer pole													
-15 < T < 15	78	7	6	86	10	8	80	10	10	100	3	3	100
-45 < T < -15	89	10	10	100	10	7	70	9	9	100	8	7	88
(B) Winter pole													
-15 < T < 15	86	11	6	55	4	3	75	14	8	57	6	3	50
-45 < T < -15	78	12	7	58	13	8	62	9	6	67	4	4	100
Totals (omitting *)													
summer	346			88			64			81			64
winter	164			57			65			61			70
-15 < T < 15	247			67			63			70			55
-45 < T < -45	263			83			66			77			71

*Biased by omission of complex boundaries

TABLE 2: Tests of statements 1-4 regarding the dependence of polar cap peak magnitudes on $\underset{\sim}{B}_{ip}$

1. Southward $\underset{\sim}{B}_{ip}$ increases the peak magnitude of E in the polar cap.
2. Northward $\underset{\sim}{B}_{ip}$ decreases " " " " " " " " " .
3. Strong $\underset{\sim}{B}_{ip}$ increases " " " " " " " " " .
4. Weak $\underset{\sim}{B}_{ip}$ decreases " " " " " " " " " .

Peak magnitudes for $\theta < -30°$, $\theta > 30°$, $B > 8\gamma$, and $B < 4\gamma$ compared with average peak magnitudes for passes between 18 ± 1^h and 6 ± 1^h MLT

	N Total	N $\theta < -30°$	agree	%	N $\theta > 30°$	agree	%	N B>8	agree	%	N B<4	agree	%
Summer Pole													
(A) for $90° < \phi < 180°$													
$-15 < T < 15$	27	2	1	50	2	2	100	3	3	100	1	1	100
$-45 < T < -15$	28	3	2	67	4	3	75	1	1	100	1	1	100
(B) for $270° < \phi < 360°$													
$-15 < T < 15$	15	3	3	100	2	2	100	4	4	100	1	1	100
$-45 < T < -15$	20	5	2	40	2	1	50	4	2	50	3	2	67
Winter Pole													
(A) for $90° < \phi < 180°$													
$-15 < T < 15$	23	3	3	100	0	-	-	2	2	100	2	1	50
$-45 < T < -15$	23	3	2	67	2	1	50	1	1	100	0	-	-
(B) for $270° < \phi < 360°$													
$-15 < T < 15$	20	3	0	0	1	1	100	5	2	40	2	1	50
$-45 < T < -15$	17	3	1	33	3	1	33	4	2	50	2	1	50
Totals													
summer	90			62			80			83			83
winter	83			50			50			58			50
$90° < \phi < 180°$	101			73			75			100			75
$270° < \phi < 360°$	72			43			63			59			63
$-15 < T < 15$	85			64			100			79			67
$-45 < T < -15$	88			50			55			60			67

TABLE 3: Tests of statements 1-4 regarding the dependence of auroral belt peak magnitudes on B_{ip}

1. Southward B_{ip} increases the peak magnitudes of E in the evening and morning auroral belts.
2. Northward B_{ip} decreases " " " " " " " " " " " " .
3. Strong B_{ip} increases " " " " " " " " " " " " .
4. Weak B_{ip} decreases " " " " " " " " " " " " .

Peak magnitudes for $\theta < -30°$, $\theta > 30°$, $B > 8^{\gamma}$, and $B < 4^{\gamma}$ compared with average peak magnitudes for passes between 18 ± 1^h and 6 ± 1^h MLT

	N Total	N $\theta < -30°$	agree	%	N $\theta > 30°$	agree	%	N B>8	agree	%	N B<4	agree	%
Summer Pole													
(A) for $90° < \phi < 180°$													
$-15 < T < 15$	54	4	2	50	4	0	0	6	4	67	2	2	100
$-45 < T < -15$	56	5	2	40	7	3	43	2	1	50	4	4	100
(b) for $270° < \phi < 360°$													
$-15 < T < 15$	31	5	5	100	5	5	100	6	6	100	2	2	100
$-45 < T < -15$	41	10	10	100	4	3	75	7	6	86	6	6	100
Winter Pole													
(A) for $90° < \phi < 180°$													
$-15 < T < 15$	44	6	3	50	0	-	-	3	1	33	2	2	100
$-45 < T < -15$	40	5	3	60	3	2	67	1	0	0	0	-	-
(B) for $270° < \phi < 360°$													
$-15 < T < 15$	35	6	5	83	1	1	100	8	4	50	4	4	100
$-45 < T < -15$	29	7	3	43	5	3	60	6	4	67	4	4	100
Totals													
summer	182			79			55			81			100
winter	148			58			67			50			100
$90° < \phi < 180°$	194			50			36			50			100
$270° < \phi < 360°$	136			82			80			74			100
$-15 < T < 15$	164			71			60			65			100
$-45 < T < -15$	166			67			58			69			100

TABLE 4:

Average Peak Magnitudes
for passes between 18 ± 1^h and 6 ± 1^h MLT
(Units: millivolts/meter)

	Polar Cap	Evening Auroral Belt	Morning Auroral Belt
Summer Hemisphere			
(A) for $90° < \phi < 180°$	40.7	36.3	40.4
(B) for $270° < \phi < 360°$	38.2	48.6	60.1
Winter Hemisphere			
(A) for $90° < \phi < 180°$	53.4	76.7	75.9
(B) for $270° < \phi < 360°$	61.5	75.9	90.9

TABLE 5: Summary of correlations with θ and $|B|$ found by comparing conditions for $B < 4\gamma$, $B > 8\gamma$, $\theta > 30^\circ$, and $\theta < -30^\circ$ with averages

Significant Correlations

1. The latitude of the low latitude boundary of the summer auroral belt E-field responds to both θ and $|B|$.

2. Peak magnitudes in the summer auroral belt respond to both θ and $|B|$ when $\underset{\sim}{B}_{ip}$ is in the sector $270^\circ < \phi < 360^\circ$.

3. Peak magnitudes of the summer polar cap E-field are influenced by the simultaneous (i.e., $-15^m < T < 15^m$) values of θ and $|B|$. In the winter polar cap this appears to be true for $90^\circ < \phi < 180^\circ$ but not for $270^\circ < \phi < 360^\circ$.

Weaker Correlations

4. There is a tendency for the latitude of the low latitude boundary of the winter auroral belt E-field to correlate with θ and $|B|$.

5. The latitude of the polar cap-auroral belt boundary in the summer hemisphere appears to be influenced by the θ angle which existed prior to the E-field measurements (i.e., at $-45^m < T < -15^m$).

Lack of Correlation

6. The latitude of the polar cap-auroral belt boundary appears to be independent of the simultaneous (i.e., $-15^m < T < 15^m$) values of θ and $|B|$.

7. Peak magnitudes in the polar cap appear to be independent of the prior (i.e., $-45^m < T < -15^m$) values of θ and $|B|$ with the exception of the summer polar cap for $90^\circ < \phi < 180^\circ$.

8. Peak magnitudes in the auroral belt appear to be independent of θ for $\underset{\sim}{B}_{ip}$ in the sector $90^\circ < \phi < 180^\circ$.

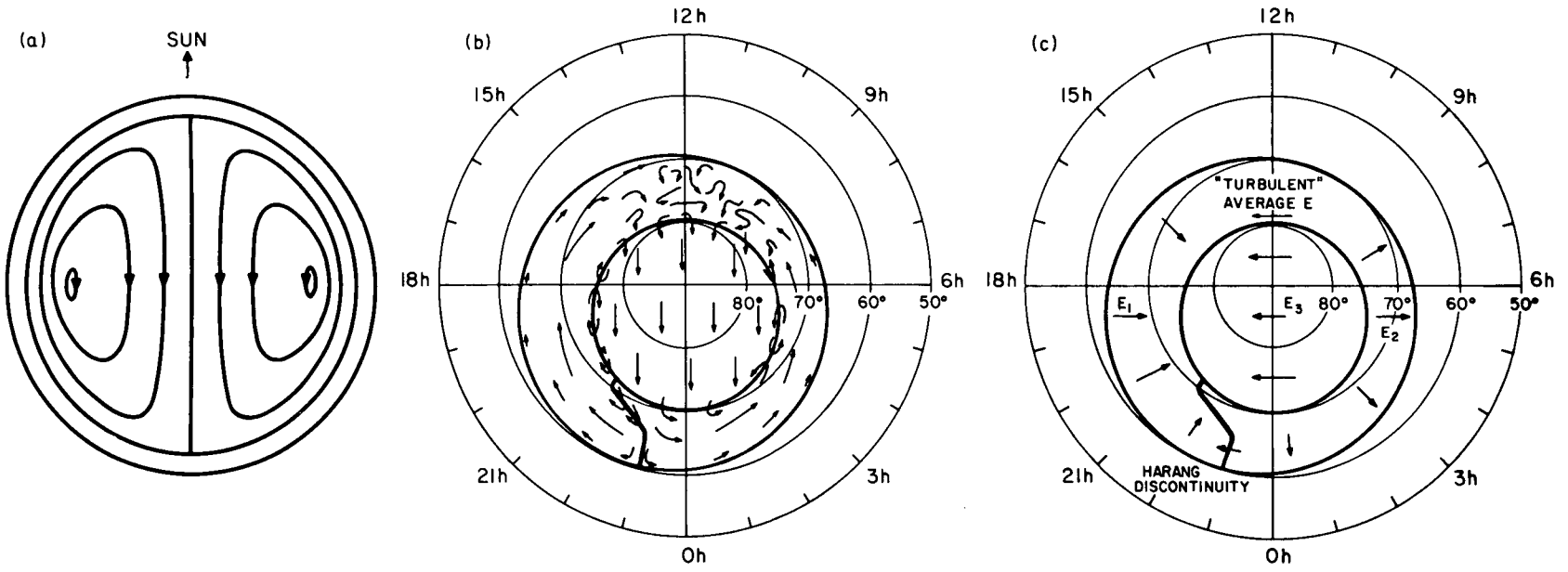
(a)
SUN
(b)
12h
15h
9h
18h
6h
21h
3h
0h
80°
70°
60°
50°
(c)
12h
15h
9h
"TURBULENT"
AVERAGE E
18h
6h
E1
E3
80°
70°
60°
50°
E2
21h
3h
HARANG
DISCONTINUITY
0h

Figure 1

36

ANTI-CORRELATED DISTRIBUTION OF THE DAWN-DUSK ELECTRIC FIELD ACROSS THE SOUTHERN AND NORTHERN POLAR CAPS

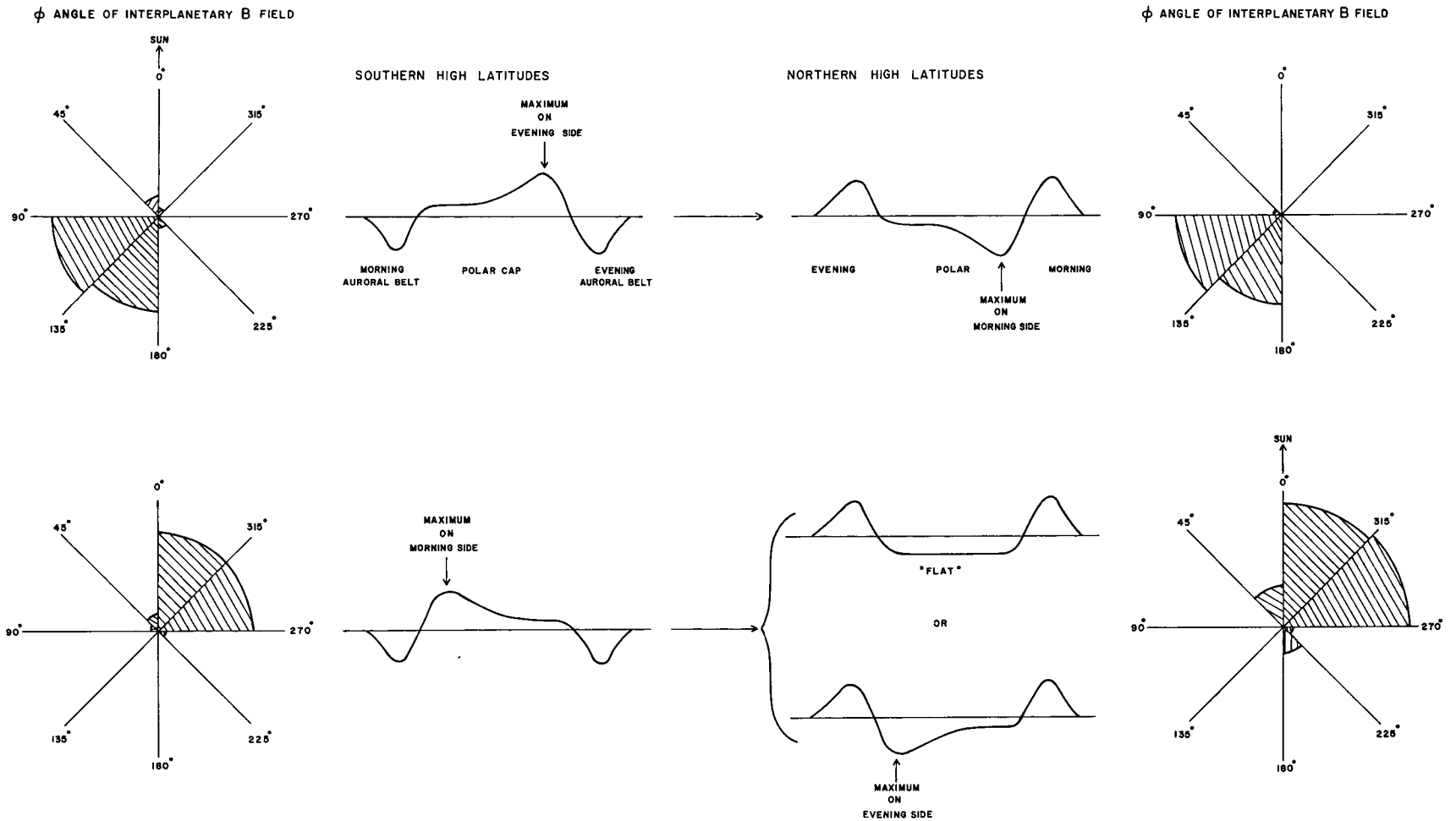

Figure 2

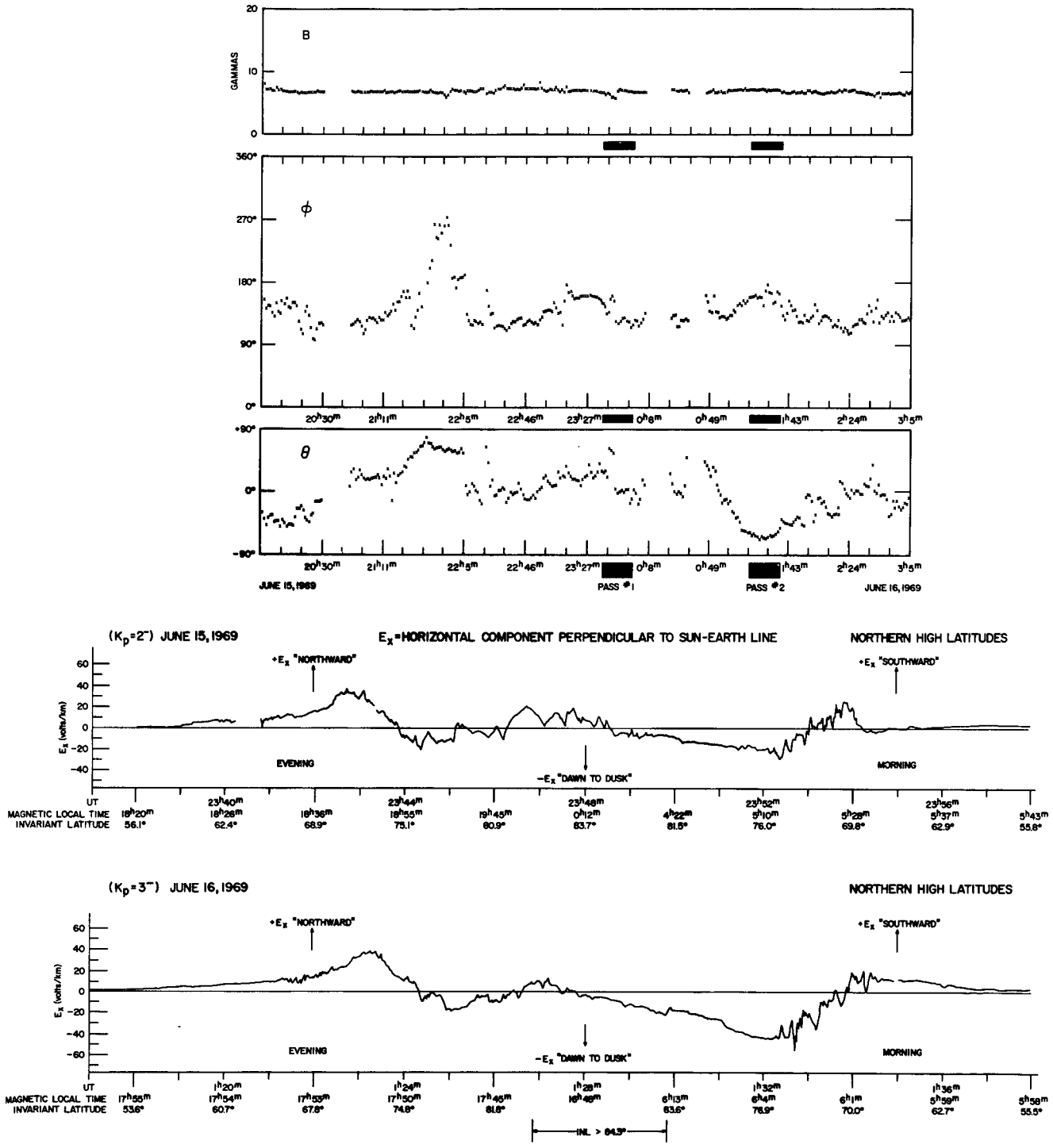
B
GAMMAS
20
10
0
360°
270°
180°
90°
0°
+90°
0°
-90°
20h30m
21h11m
22h5m
22h46m
23h27m
0h8m
0h49m
1h43m
2h24m
3h5m
JUNE 15, 1969
PASS #1
PASS #2
JUNE 16, 1969
(Kp=2⁻) JUNE 15, 1969
Ex=HORIZONTAL COMPONENT PERPENDICULAR TO SUN-EARTH LINE
NORTHERN HIGH LATITUDES
+Ex "NORTHWARD"
+Ex "SOUTHWARD"
Ex (volts/km)
EVENING
-Ex "DAWN TO DUSK"
MORNING
UT
MAGNETIC LOCAL TIME
INVARIANT LATITUDE
18h20m 56.1°
23h40m 18h28m 62.4°
18h36m 68.9°
23h44m 18h55m 75.1°
19h45m 80.9°
23h48m 0h12m 83.7°
4h22m 81.5°
23h52m 5h10m 76.0°
5h28m 69.8°
23h56m 5h37m 62.9°
5h43m 55.8°
(Kp=3⁻) JUNE 16, 1969
NORTHERN HIGH LATITUDES
+Ex "NORTHWARD"
+Ex "SOUTHWARD"
Ex (volts/km)
EVENING
-Ex "DAWN TO DUSK"
MORNING
UT
MAGNETIC LOCAL TIME
INVARIANT LATITUDE
17h55m 53.6°
1h20m 17h54m 60.7°
17h53m 67.8°
1h24m 17h50m 74.8°
17h45m 81.8°
1h28m 18h48m 83.6°
6h13m 83.6°
1h32m 6h4m 76.9°
6h1m 70.0°
1h36m 5h59m 62.7°
5h58m 55.5°
INL > 84.3°

Figure 3

38

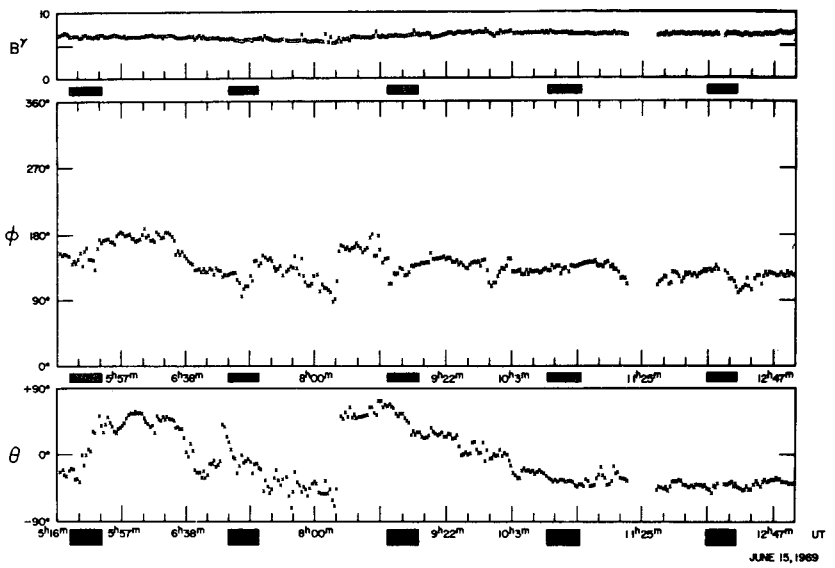
B^Y
φ
θ
JUNE 15, 1969

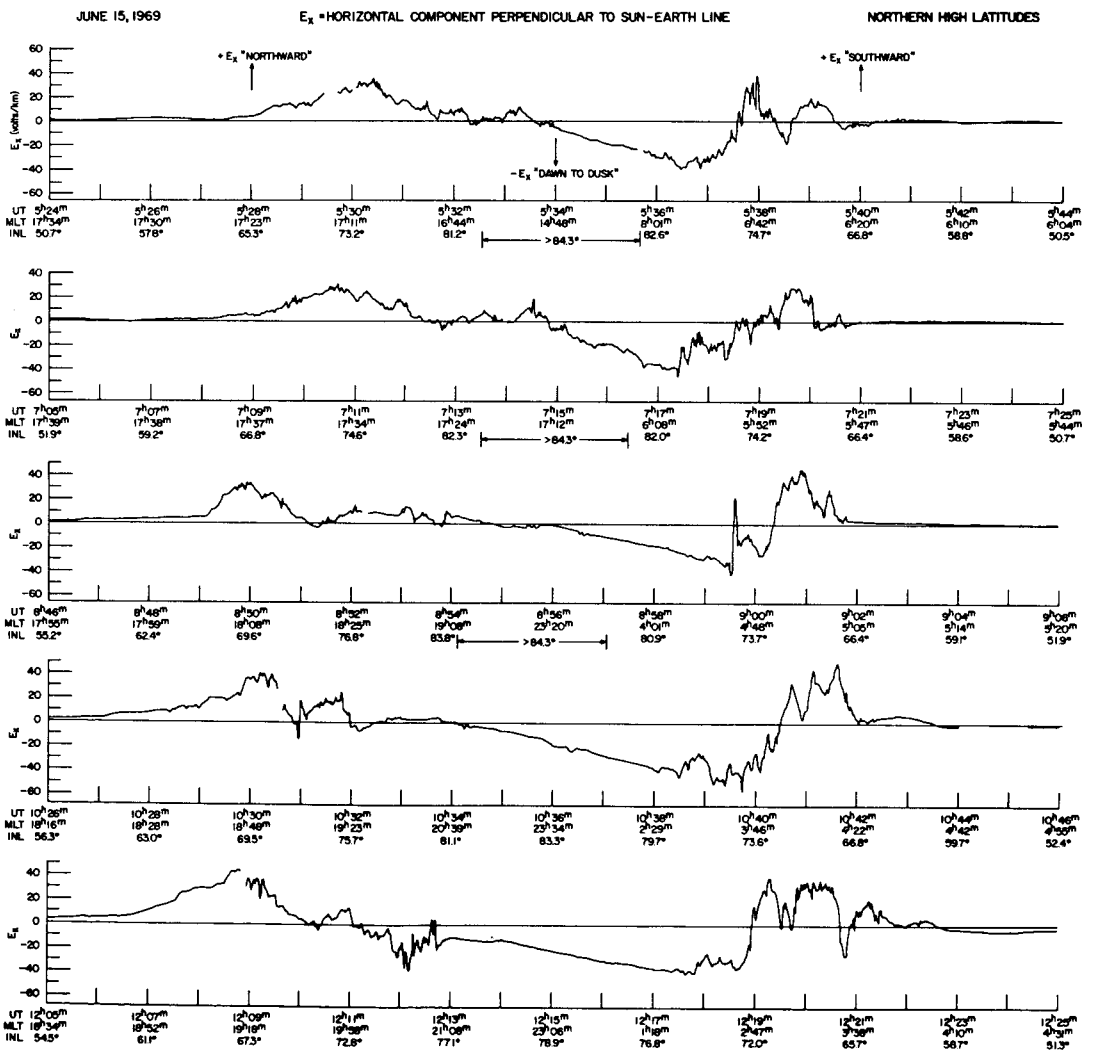
JUNE 15, 1969
E_x = HORIZONTAL COMPONENT PERPENDICULAR TO SUN-EARTH LINE
NORTHERN HIGH LATITUDES
+E_x "NORTHWARD"
+E_x "SOUTHWARD"
-E_x "DAWN TO DUSK"
E_x (volts/km)
UT
MLT
INL
>84.3°

Figure 4

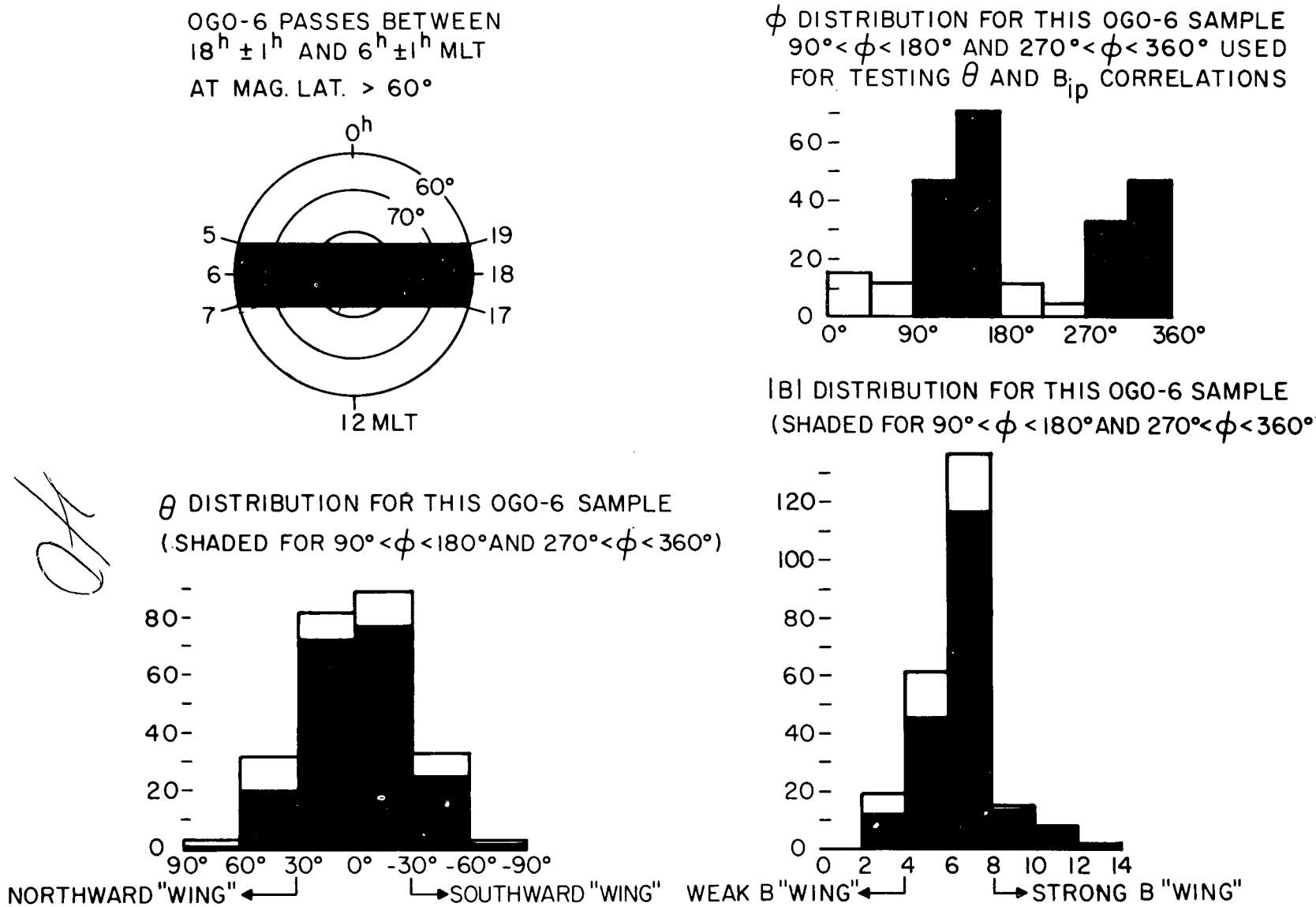
OGO-6 PASSES BETWEEN
18h ± 1h AND 6h ± 1h MLT
AT MAG. LAT. > 60°
0h
60°
70°
5
6
7
19
18
17
12 MLT
φ DISTRIBUTION FOR THIS OGO-6 SAMPLE
90°< φ <180° AND 270°< φ <360° USED
FOR TESTING θ AND Bip CORRELATIONS
60
40
20
0
0°
90°
180°
270°
360°
|B| DISTRIBUTION FOR THIS OGO-6 SAMPLE
(SHADED FOR 90°< φ <180° AND 270°< φ <360°)
120
100
80
60
40
20
0
0 2 4 6 8 10 12 14
WEAK B "WING"
STRONG B "WING"
θ DISTRIBUTION FOR THIS OGO-6 SAMPLE
(SHADED FOR 90°< φ <180° AND 270°< φ <360°)
80
60
40
20
0
90° 60° 30° 0° -30° -60° -90°
NORTHWARD "WING"
SOUTHWARD "WING"

Figure 5

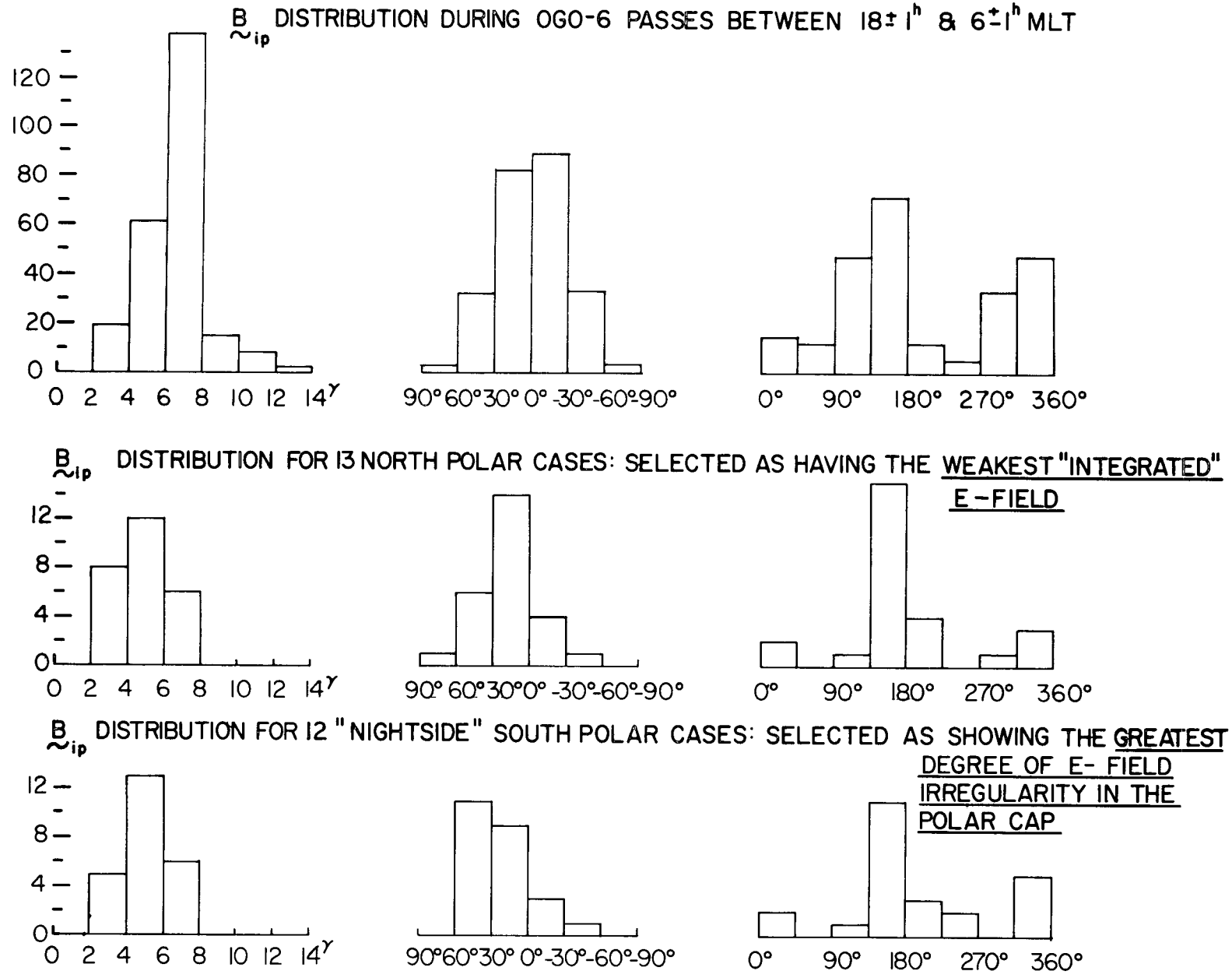

Figure 6

NASA-GSFC